

## Mode-Locked Ultrashort Pulse Generation from On-Chip Normal Dispersion Microresonators

S.-W. Huang,<sup>1,2,\*</sup> H. Zhou,<sup>2</sup> J. Yang,<sup>1,2</sup> J. F. McMillan,<sup>2</sup> A. Matsko,<sup>3</sup> M. Yu,<sup>4</sup> D.-L. Kwong,<sup>4</sup> L. Maleki,<sup>3</sup> and C. W. Wong<sup>1,2,†</sup>

<sup>1</sup>*Mesoscopic Optics and Quantum Electronics, University of California, Los Angeles, California 90095, USA*

<sup>2</sup>*Optical Nanostructures Laboratory, Center for Integrated Science and Engineering, Solid-State Science and Engineering, and Mechanical Engineering, Columbia University, New York, New York 10027, USA*

<sup>3</sup>*OEwaves Inc., Pasadena, California 91107, USA*

<sup>4</sup>*Institute of Microelectronics, Singapore 117685, Singapore*

(Received 14 March 2014; published 4 February 2015)

We describe generation of stable mode-locked pulse trains from on-chip normal dispersion microresonators. The excitation of hyperparametric oscillation is facilitated by the local dispersion disruptions induced by mode interactions. The system is then driven from hyperparametric oscillation to the mode-locked state with over 200 nm spectral width by controlled pump power and detuning. With the continuous-wave-driven nonlinearity, the pulses sit on a pedestal, akin to a cavity soliton. We identify the importance of pump detuning and wavelength-dependent quality factors in stabilizing and shaping the pulse structure, to achieve a single pulse inside the cavity. We examine the mode-locking dynamics by numerically solving the master equation and provide analytic solutions under appropriate approximations.

DOI: 10.1103/PhysRevLett.114.053901

PACS numbers: 42.65.Re, 42.55.Sa, 42.65.Hw, 42.65.Yj

Recently, continuous-wave pumped monolithic microresonators have emerged as promising platforms for compact optical (Kerr) frequency comb generation [1–11]. With anomalous group-velocity dispersion (GVD) and self-phase modulation, optical solitons can be generated [12,13], and remarkably broad bandwidths [6] and rf-optical stability [3] have been demonstrated. Obtaining anomalous GVD broadly across arbitrary pump frequencies, however, is challenging for microresonators [14]. Dispersion engineering by conformal coating [15–17] and waveguide shaping [18] is possible, but often lead to lower quality factors ( $Q$ ). Alternatively, frequency comb and ultrashort pulse generation from normal GVD microresonators has been theoretically predicted [19–21] and comblike spectra from normal GVD crystalline resonators were recently measured [22,23]. Further investigation into this normal GVD architecture, especially in the time domain and that of coherent mode locking, will open up new fields in chip-scale oscillators, waveform generation, and ultrafast spectroscopy.

Here we report mode-locked pulse generation from on-chip normal dispersion microresonators. The observation is supported by phase noise characterization, frequency-resolved optical gating (FROG) pulse measurement, and numerical modeling [24,25]. The phase retrieval from the FROG measurement reveals a pulse structure akin to a cavity soliton: a 74 fs mode-locked pulse sitting on a cw background. Numerical modeling of the cw-driven nonlinear microresonator, capturing the full spectra with the measured GVD and  $Q$ 's, confirms the feasibility of mode-locked pulse generation and agrees with our measurements. We demonstrate, both experimentally and numerically, the importance of pump detuning and wavelength-dependent  $Q$  factors in stabilizing and shaping the pulses generated from the normal GVD

microresonators. Finally, we obtain the closed-form solution of the master equation under appropriate approximations, showing explicitly the connection between the microresonator parameters and the mode-locked pulse properties.

Figure 1(a) is the transmission of our  $\text{Si}_3\text{N}_4$  microring resonator. Five modal families (3 TE and 2 TM) are identified from the transmission, and each Lorentzian resonance is fitted to determine its frequency and  $Q$  factor [26]. The frequency data are then used to evaluate the GVD. For the fundamental mode family, a loaded  $Q$  factor of more than  $10^6$  is achieved at 1600 nm while the  $Q$  factors at the telecommunications C-band wavelengths are more than 4 times lower due to residual N-H absorption [27]. For the higher-order mode families,  $Q$  factors are orders of magnitude smaller and thus no Kerr comb is generated from these mode families.  $Q$  factors are also reduced at longer than 1625 nm due to increasing coupling loss. Therefore, the resonator has a distinct spectrally restricted area characterized with the highest  $Q$  factor. As discussed later, this feature is critical for the mode-locked pulse generation in our normal GVD microresonators. Figure 1(b) shows the measured fundamental mode dispersion of our ring resonator, in good agreement with our numerical modeling using a full-vectorial finite-element mode solver. Across the whole  $L$  band, the fundamental mode features a normal GVD with local disruptions induced by fundamental mode family interaction with the higher-order modes. Such change of local GVD facilitates the start of the hyperparametric oscillation from our microresonator [26]. An example Kerr comb spectrum is shown in Fig. 1(c), with a spectral width spanning more than 200 nm.

The optical spectrum shows a clean mode structure with comb lines separated by single free spectral range (FSR) of the fundamental mode family, without identifiable noise

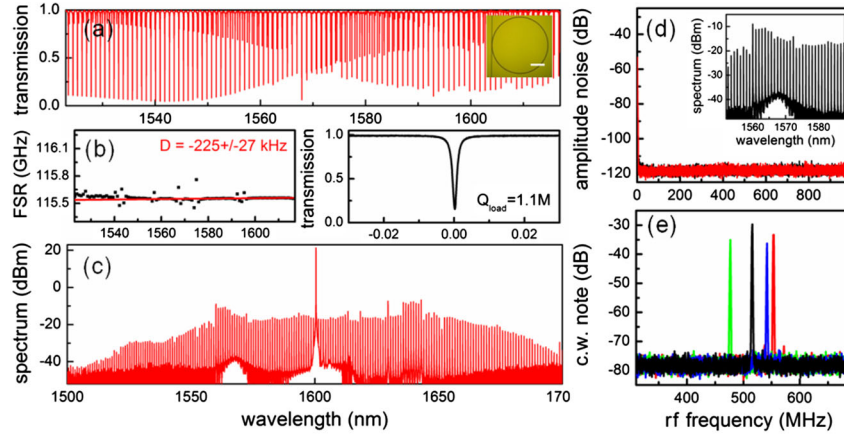


FIG. 1 (color online). (a) Transmission of the cavity modes. Inset: Optical micrograph of the ring resonator. Scale bar:  $100 \mu\text{m}$ . (b) Left: Wavelength-dependent FSR, measuring a nonequidistance of the modes,  $D_2 \equiv -\beta_2 c \omega_{\text{FSR}}^2 / n_0$ , of  $-225 \text{ kHz}$ , in good agreement with the simulation result from a full-vector finite-element mode solver,  $D_2 = -270 \text{ kHz}$ . Right: Transmission of the cavity mode at the pump wavelength, measuring a quality factor of  $1.1 \times 10^6$ . (c) Example Kerr comb spectrum, with a spectral width spanning more than  $200 \text{ nm}$ . (d) rf amplitude noise of the Kerr comb (black curve) along with the detector background (red curve), indicating the low phase noise operation. Inset: Zoom-in plot of the optical spectrum, showing a clean comb structure. (e) cw heterodyne beat notes between a cw laser and different comb lines (black, pump; blue, 10th mode; red, 20th mode; green, 21st mode). No linewidth broadening of the comb lines relative to the pump is observed, showing the comb retains a similar level of phase noise as the cw laser.

peaks between comb lines [Fig. 1(d), inset]. We investigated the Kerr comb coherence by measuring the rf amplitude noise with a scan range much larger than the cavity linewidth and by performing a cw heterodyne beat note measurement [28,29]. Both measurements confirmed the coherence of the Kerr comb. The use of rf amplitude noise as a measure of low phase noise operation has been demonstrated and widely employed [13,28,29]. With proper change of the pump power and detuning, the Kerr comb is driven into the low phase noise regime as shown in Fig. 1(d). The cw heterodyne beat note measurements are shown in Fig. 1(e). In addition to the beat note of the cw laser with the pump laser, beat notes between the cw laser and different comb lines are also measured. All beat notes exhibit the same linewidth of  $800 \text{ kHz}$ , limited by coherence between the cw laser and the pump laser. Neither additional linewidth broadening of the comb lines relative to the pump nor multiple beat notes were observed, confirming that the comb lines exhibit a similar level of phase noise as the pump.

We measured the pulse duration via subfemtjoule sensitive SHG noncollinear FROG [30,31] without involvement of any optical amplification nor external bandpass filtering, to minimize pulse distortion. Careful checks were conducted to ensure no interferometric second-harmonic signal was collected in the FROG spectrogram [32]. Figure 2(a) is the spectrogram with  $32 \text{ ps}$  delay scan. It shows a pulse train with  $8.7 \text{ ps}$  period, the inverse of the fundamental mode family FSR ( $115.56 \text{ GHz}$ ). For better visualization, Fig. 2(a) is plotted on a log-scale and the bright cw pump component is removed in the plot. Spectral interferometric fringes are clearly visible for delays longer than the pulse duration. This interference arises due to the presence of the cw background as it can also mix with the pulse, generating two temporally separated FROG signal pulses. The fringes become sparse as the delay

approaches zero and the patterns depend on the relative phase between the cw pump and the pulse [33]. Figures 2(b) and 2(c) are the spectrogram measured with a finer time resolution,  $4 \text{ fs}$ , and Fig. 2(c) is the reconstructed spectrogram with a FROG error of  $2.7\%$ . Because of the complexity of the pulses, an iterative genetic algorithm is developed specifically to retrieve the spectrograms [26]. Figure 2(d) shows the retrieved pulse shape (red curve) and temporal phase profile (blue curve), with a  $1.3 \text{ rad}$  relative phase contrast observed within the pulse. The FWHM pulse duration is measured at  $74 \text{ fs}$ , positively chirped from its transform-limited FWHM pulse duration of  $55 \text{ fs}$ . Because of the nature of the cw driven nonlinearity, the observed mode-locked pulse necessarily sits on a pedestal, analogous to a cavity soliton.

Figure 2(e) shows the measured optical intensity autocorrelation (AC) trace of the generated pulse train, and the left-hand panel of Fig. 2(f) plots the zoom-in view. Of note, this is not an interferometric autocorrelation, and thus the temporal fringes in the AC trace represent the actual oscillating structures of the pulse. Between the pulses, temporal fringes with a period of  $\sim 200 \text{ fs}$  are clearly observed and these fringes arise from the presence of the primary comb lines,  $\sim 4.85 \text{ THz}$  ( $42\text{nd}$  mode) away from the pump [26]. In addition, the right-hand panel of Fig. 2(f) shows the calculated AC traces of a stable transform-limited pulse train (black curve) and an unstable pulse train (red curve). As the instability results in the significantly increased background level of the AC trace, it shows that the instability of the generated pulse train is minimal and provides another confirmation of the stable mode-locked pulse generation [34].

To shed light on the pulse generation mechanism, we first performed numerical simulation solving the Lugiato-Lefever equation for  $512$  modes around the cw pump [25]. Experimentally measured dispersion [Fig. 1(b)] and

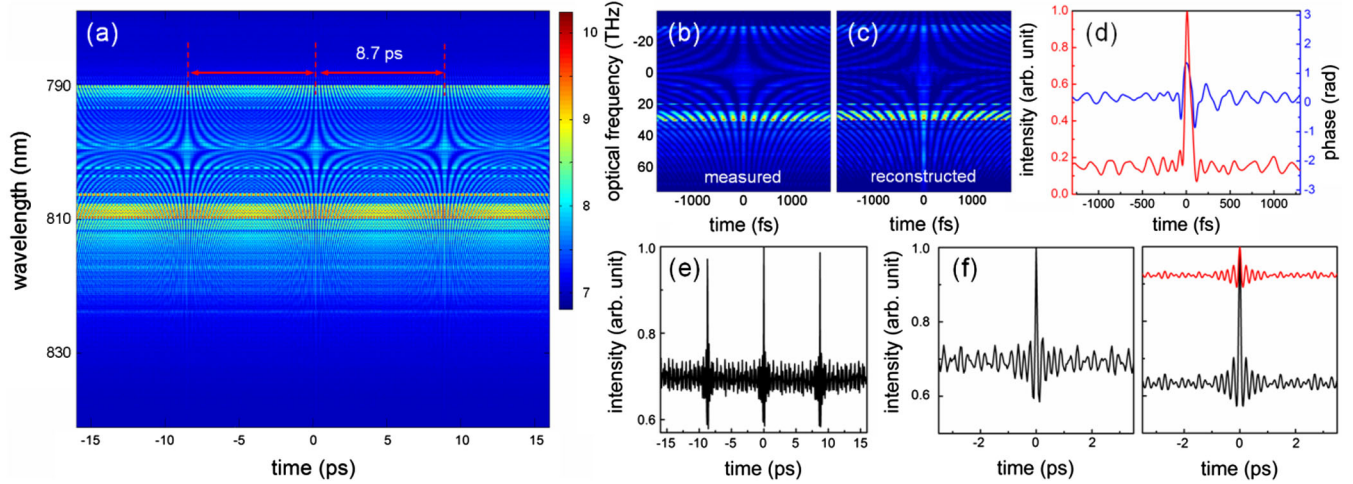


FIG. 2 (color online). (a) FROG spectrogram with a delay scan of 32 ps, showing a fundamentally mode-locked pulse train. (b) FROG spectrogram measured with a finer time resolution of 4 fs. (c) Reconstructed FROG spectrogram achieved by use of genetic algorithms. (d) Retrieved pulse shape (light curve) and temporal phase profile (dark curve), measuring a 74 fs FWHM pulse duration. (e) Measured AC of the generated fundamentally mode-locked pulse train. (f) Left: Zoom-in plot of the measured AC. Right: Calculated ACs of a transform-limited stable pulse train (dark curve) and an unstable pulse train showing a significantly larger AC background (light curve).

wavelength-dependent  $Q$  values (Fig. S2 in the Supplemental Material [26]), including the local dispersion disruptions, are entered into the modeling [26]. Figure 3(a) shows the simulation results, illustrating the emergence of the first pairs of hyperparametric oscillation sidebands around the  $\pm 42$ nd modes. A good agreement with the experimental emergence result (inset) is achieved. With the proper pump power and detuning, a fundamentally mode-locked pulse train is generated as shown in Fig. 3(b). The modeled FWHM pulse duration is 110 fs and the relative phase contrast is 1.7 rad (positively chirped), in good agreement with the FROG measurements.

Next, we numerically examined idealistic nonlinear microresonators characterized by solely normal GVDs and symmetric wavelength-dependent  $Q$  factors to elucidate the mode-locking physics [26]. Figure S14 in the Supplemental Material [26] shows the case with larger  $D_2$  of 0.03 (or  $-2.7$  MHz) and without wavelength dependence in the  $Q$  factors. A phase-locked Kerr comb can be generated, but the pulse duration is long and the shape

complex. This is because, unlike in anomalous GVD microresonators, pulse broadening due to the normal GVD is not balanced by self-phase modulation and thus an additional mechanism has to be introduced to stabilize and shape the pulses. In Fig. S15 [26], we numerically introduce wavelength-dependent  $Q$  factors, effectively a bandpass filter, and then clean mode-locked pulses are generated from the microresonator. These are dark pulses and the exact pulse shapes depend on the bandpass filter bandwidth. Next, when  $D_2$  is numerically set smaller at 0.003 (and closer to the experimental value), bright pulses can also be observed. Different from the case of large normal dispersion where only dark pulses exist, both bright and dark pulses are possible in the small normal dispersion case, depending on the exact combination of dispersion and bandpass filter bandwidth (Fig. S16 [26]). It is even possible to generate square pulses directly with the correct sets of  $Q$ -factor profile, GVD, and detuning [Fig. 3(c)]. We note that the mode-locking mechanism has analogies to, but is not identical to, the pulse generation mechanism in

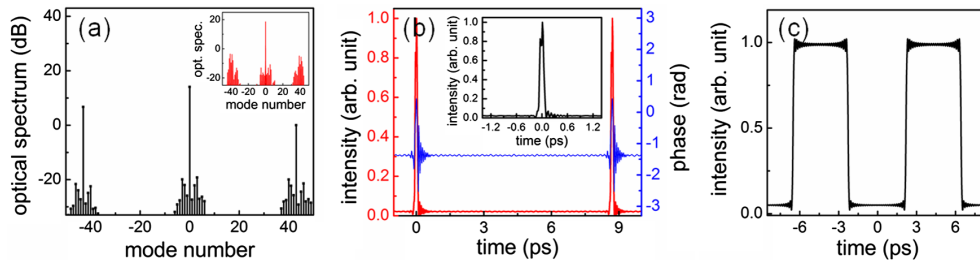


FIG. 3 (color online). (a) Near the threshold and with a small red detuning of 180 MHz, the first pairs of hyperparametric oscillation sidebands emerge at around the  $\pm 42$ nd modes, showing good agreement with the experimental result (inset). (b) With the proper pump power (260 mW) and red detuning (2.5 GHz), a mode-locked pulse train is generated. The light and dark curves are the modeled pulse shape and the temporal phase profile, respectively. Inset: Zoom-in plot of the pulse shape, showing an ultrashort FWHM pulse duration of 110 fs. (c) Square optical pulses can also be generated directly from a normal GVD microresonator. The conditions for the observation of these square pulses are  $D_2 = 0.002$ , red detuning of  $7.7\gamma_0$ , resonance linewidth of  $\gamma_j = \gamma_{j_0}[1 + 0.01(j - j_0)^2]$ , and pump power 25 times larger than the threshold.



all-normal dispersion fiber lasers [35], a variant of additive pulse mode locking [36].

To experimentally examine the effect of wavelength-dependent  $Q$  factors, we then reannealed the same microresonator at 1200 °C to reduce the absorption in the shorter wavelengths such that the  $Q$  roll-off is less pronounced (Figure S2 [26]). Figure 4(a) shows the Kerr comb generated from the reannealed microresonator, showing a smoother and broader spectrum than the one shown in Fig. 1(c). Similarly, the comb can be driven into a low phase noise state [Fig. 4(b)]. However, now without the effective narrow bandpass filter, mode-locked pulses are not observed as evidenced by the high background level ( $\approx 0.85$ ) in the AC trace. A phase stable state without mode locking is also observed in another recent study using a different microresonator platform [37].

Furthermore, we seek the closed-form solution of the master equation for the Kerr comb and pulse generation:

$$\begin{aligned} T_R \frac{\partial}{\partial T} A + \frac{i}{2} \left( \beta_{2\Sigma} + i \frac{T_c}{\Omega_f^2} \right) \frac{\partial^2}{\partial t^2} A - i\gamma |A|^2 A \\ = - \left( \alpha + \frac{T_c}{2} + i\delta_0 \right) A + i\sqrt{T_c P_{\text{in}}} e^{i\varphi_{\text{in}}}, \end{aligned} \quad (1)$$

where  $A(T, t)$  is the microresonator electric field slowly varying envelope,  $T_R$  the cavity round-trip time,  $t$  the retarded time,  $T$  the slow time of the cavity,  $\beta_{2\Sigma}$  the cavity GVD,  $T_c$  the power coupling loss per round-trip,  $\Omega_f$  the spectral characteristics of the coupling,  $\gamma$  the nonlinear coefficient,  $\alpha$  the amplitude attenuation per round-trip,  $\delta_0$  the resonance detuning, and  $\sqrt{P_{\text{in}}} e^{i\varphi_{\text{in}}}$  the cw pump. Here, for simplicity, we assume the intracavity bandpass filter results solely from wavelength-dependent coupling loss:  $T_{\text{coupling}} \approx T_c [1 + ((\omega_c - \omega)^2 / \Omega_f^2)]$ , where  $\omega_c$  is the frequency for maximal coupling. Assuming Gaussian input pulse and applying the variational method, the equations describing the mode-locked pulses are derived in Eq. (S9) [26]. Defining chirp  $q$ , pulse energy  $E_p$ , and the pulse duration  $\tau$ , and with  $q^2 \gg \Omega_f^2 \tau^2 \gg 1$ , we obtain the resulting solutions:

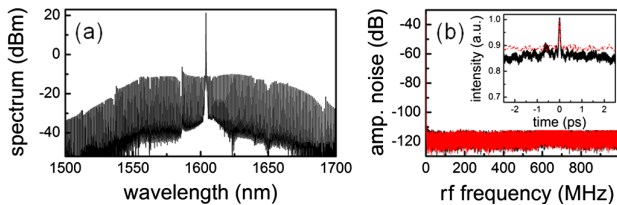


FIG. 4 (color online). (a) Example Kerr comb spectrum from the reannealed microresonator, showing a smoother and broader spectrum. (b) rf amplitude noise of the Kerr comb (black curve) along with the detector background (red curve). While the Kerr comb can also be driven to a low phase noise state, the high background level of the AC trace (inset) indicates the absence of mode-locked pulses. The red dashed line is the calculated AC trace assuming random spectral phases.

$$E_p \approx \frac{8\sqrt{10\pi} \beta_{2\Sigma}^{3/2} \Omega_f^2 \sqrt{\delta_0}}{15 T_c \gamma}, \quad (2)$$

$$\tau \approx \frac{2\sqrt{5} \beta_{2\Sigma}^{3/2} \Omega_f^2}{3 T_c \sqrt{\delta_0}}, \quad (3)$$

$$q \approx \frac{4\beta_{2\Sigma} \Omega_f^2}{3T_c}. \quad (4)$$

By fitting the measured  $Q$  factor (Fig. S2 [26]) of the  $\pm 20$  modes around  $Q_{\text{max}}$  with the wavelength-dependent coupling loss profile defined above, a filter bandwidth of 2.3 THz is found. A chirp  $q$  of 1.6 is then obtained after the filter bandwidth and the other measured parameters ( $T_c = 0.003$ ,  $\beta_{2\Sigma} = 17.14$  fs<sup>2</sup>) are entered into Eq. (4). This chirp is close to that obtained from the FROG measurement ( $q = 1.5$ ), and the resulting calculated FWHM pulse duration (98 fs) is close to our measurements.

While the total power in the microresonator reduces as the pump detuning gets larger, Eqs. (2) and (3) show that the pulse energy actually increases and the pulse duration gets shorter. Overall, the pulse quality improves. It illustrates the active role of pump detuning: it is not simply a parameter that controls the coupled power in the microresonator, but an important physical factor that determines the pulse duration and energy distribution between the pulse and cw background. Furthermore, the closed-form solutions show that the pulse generated from a normal GVD microresonator is always chirped [Eq. (4)], and a narrower bandpass filter is necessary to keep the pulse short when the dispersion increases.

In summary, we report on observations of direct generation of pulses from on-chip normal dispersion microresonator, supported by phase noise characterization, FROG pulse measurement, and numerical modeling. The excitation of the hyperparametric oscillation is facilitated by the local dispersion disruptions induced by mode interactions. Then the system is driven from the hyperparametric oscillation to the mode-locked pulse generation by a proper change of the pump power and detuning. The phase retrieval from the FROG measurement reveals a 74 fs fundamentally mode-locked pulse sitting on a cw background. Numerical modeling of the cw-driven nonlinear microresonator, capturing the full spectra with the measured GVD and  $Q$ 's, confirms the feasibility of mode-locked pulse generation and agrees with our measurements. We show, both experimentally and numerically, the importance of pump detuning and effective bandpass filtering (resulting from wavelength dependent  $Q$ -factor of the resonator) in stabilizing and shaping the pulses generated from normal GVD microresonators. Finally, we present the closed-form solution of the master equation under appropriate approximations, facilitating the design of mode-locked pulse generation from microresonators.

The authors acknowledge discussions with Erich P. Ippen, Zhenda Xie, and Jiangjun Zheng, a spectroscopic ellipsometer measurement and analysis at Brookhaven National Laboratory by Felice Gesuele and Tingyi Gu,

respectively, and loan of the  $L$ -band EDFA and the rf spectrum analyzer from the Bergman and Shepard groups at Columbia, respectively. We acknowledge support from ONR and DARPA on this study.

\*swhuang@seas.ucla.edu

†cheewei.wong@ucla.edu

- [1] P. Del'Haye, A. Schliesser, O. Arcizet, T. Wilken, R. Holzwarth, and T. J. Kippenberg, *Nature (London)* **450**, 1214 (2007).
- [2] A. A. Savchenkov, A. B. Matsko, V. S. Ilchenko, I. Solomatine, D. Seidel, and L. Maleki, *Phys. Rev. Lett.* **101**, 093902 (2008).
- [3] P. Del'Haye, O. Arcizet, A. Schliesser, R. Holzwarth, and T. J. Kippenberg, *Phys. Rev. Lett.* **101**, 053903 (2008).
- [4] J. S. Levy, A. Gondarenko, M. A. Foster, A. C. Turner-Foster, A. L. Gaeta, and M. Lipson, *Nat. Photonics* **4**, 37 (2010).
- [5] L. Razzari, D. Duchesne, M. Ferrera, R. Morandotti, S. Chu, B. E. Little, and D. J. Moss, *Nat. Photonics* **4**, 41 (2010).
- [6] Y. Okawachi, K. Saha, J. S. Levy, Y. H. Wen, M. Lipson, and A. L. Gaeta, *Opt. Lett.* **36**, 3398 (2011).
- [7] T. J. Kippenberg, R. Holzwarth, and S. A. Diddams, *Science* **332**, 555 (2011).
- [8] F. Ferdous, H. Miao, D. E. Leaird, K. Srinivasan, J. Wang, L. Chen, L. T. Varghese, and A. M. Weiner, *Nat. Photonics* **5**, 770 (2011).
- [9] M. A. Foster, J. S. Levy, O. Kuzucu, K. Saha, M. Lipson, and A. L. Gaeta, *Opt. Express* **19**, 14233 (2011).
- [10] M. Peccianti, A. Pasquazi, Y. Park, B. E. Little, S. T. Chu, D. J. Moss, and R. Morandotti, *Nat. Commun.* **3**, 765 (2012).
- [11] F. Ferdous, H. Miao, P.-H. Wang, D. E. Leaird, K. Srinivasan, L. Chen, V. Aksyuk, and A. M. Weiner, *Opt. Express* **20**, 21033 (2012).
- [12] T. Herr, V. Brasch, J. D. Jost, C. Y. Wang, N. M. Kondratiev, M. L. Gorodetsky, and T. J. Kippenberg, *Nat. Photonics* **8**, 145 (2014).
- [13] K. Saha, Y. Okawachi, B. Shim, J. S. Levy, R. Salem, A. R. Johnson, M. A. Foster, M. R. E. Lamont, M. Lipson, and A. L. Gaeta, *Opt. Express* **21**, 1335 (2013).
- [14] D. J. Moss, R. Morandotti, A. L. Gaeta, and M. Lipson, *Nat. Photonics* **7**, 597 (2013).
- [15] J. Riemensberger, K. Hartinger, T. Herr, V. Brasch, R. Holzwarth, and T. J. Kippenberg, *Opt. Express* **20**, 27661 (2012).
- [16] V. S. Ilchenko, A. A. Savchenkov, A. B. Matsko, and L. Maleki, *J. Opt. Soc. Am. A* **20**, 157 (2003).
- [17] C. J. Chen, C. A. Husko, I. Meric, K. L. Shepard, C. W. Wong, W. M. J. Green, Y. A. Vlasov, and S. Assefa, *Appl. Phys. Lett.* **96**, 081107 (2010).
- [18] L. Zhang, C. Bao, V. Singh, J. Mu, C. Yang, A. M. Agarwal, L. C. Kimmerling, and J. Michel, *Opt. Lett.* **38**, 5122 (2013).
- [19] A. B. Matsko, A. A. Savchenkov, and L. Maleki, *Opt. Lett.* **37**, 43 (2012).
- [20] T. Hansson, D. Modotto, and S. Wabnitz, *Phys. Rev. A* **88**, 023819 (2013).
- [21] C. Godey, I. V. Balakireva, A. Coillet, and Y. K. Chembo, *Phys. Rev. A* **89**, 063814 (2014).
- [22] A. Coillet, I. Balakireva, R. Henriet, K. Saleh, L. Larger, J. M. Dudley, C. R. Menyuk, and Y. K. Chembo, *IEEE Photon. J.* **5**, 6100409 (2013).
- [23] I. S. Grudin, L. Baumgartel, and N. Yu, *Opt. Express* **21**, 26929 (2013).
- [24] Y. K. Chembo and N. Yu, *Phys. Rev. A* **82**, 033801 (2010).
- [25] S. Coen, H. G. Randle, T. Sylvestre, and M. Erkintalo, *Opt. Lett.* **38**, 37 (2013).
- [26] See Supplemental Material at <http://link.aps.org/supplemental/10.1103/PhysRevLett.114.053901> for device fabrication, characterization and analysis methods, numerical simulation, and derivation of analytic solution, which includes Refs. [38–52].
- [27] R. Germann, H. W. M. Salemink, R. Beyeler, G. L. Bona, F. Horst, I. Massarek, and B. J. Offrein, *J. Electrochem. Soc.* **147**, 2237 (2000).
- [28] T. Herr, K. Hartinger, J. Riemensberger, C. Y. Wang, E. Gavartin, R. Holzwarth, M. L. Gorodetsky, and T. J. Kippenberg, *Nat. Photonics* **6**, 480 (2012).
- [29] C. Y. Wang, T. Herr, P. Del'Haye, A. Schliesser, J. Hofer, R. Holzwarth, T. W. Hänsch, N. Picqué, and T. J. Kippenberg, *Nat. Commun.* **4**, 1345 (2013).
- [30] R. Trebino, *Frequency-Resolved Optical Gating: The Measurement of Ultrashort Laser Pulses* (Springer, New York, 2000).
- [31] C. A. Husko, S. Combrié, P. Colman, J. Zheng, A. D. Rossi, and C. W. Wong, *Sci. Rep.* **3**, 1100 (2013).
- [32] G. Stübgen and G. Steinmeyer, *Opt. Express* **13**, 2617 (2005).
- [33] J. K. Jang, M. Erkintalo, S. G. Murdoch, and S. Coen, *Nat. Photonics* **7**, 657 (2013).
- [34] M. Rhodes, G. Steinmeyer, J. Ratner, and R. Trebino, *Laser Photonics Rev.* **7**, 557 (2013).
- [35] A. Chong, W. H. Renninger, and F. W. Wise, *J. Opt. Soc. Am. B* **25**, 140 (2008).
- [36] H. A. Haus, J. G. Fujimoto, and E. P. Ippen, *J. Opt. Soc. Am. B* **8**, 2068 (1991).
- [37] P. Del'Haye, K. Beha, S. B. Papp, and S. A. Diddams, *Phys. Rev. Lett.* **112**, 043905 (2014).
- [38] J. Riemensberger, K. Hartinger, T. Herr, V. Brasch, R. Holzwarth, and T. J. Kippenberg, *Opt. Express* **20**, 27661 (2012).
- [39] S. L. Gilbert, W. C. Swann, and C. M. Wang, *Natl. Inst. Stand. Technol. Spec. Publ.* **260**, 137 (1998).
- [40] P. Del'Haye, O. Arcizet, M. L. Gorodetsky, R. Holzwarth, and T. J. Kippenberg, *Nat. Photonics* **3**, 529 (2009).
- [41] A. Arbabi and L. L. Goddard, *Opt. Lett.* **38**, 3878 (2013).
- [42] C.-L. Tien and T.-W. Lin, *Appl. Opt.* **51**, 7229 (2012).
- [43] A. A. Savchenkov, A. B. Matsko, W. Liang, V. S. Ilchenko, D. Seidel, and L. Maleki, *Opt. Express* **20**, 27290 (2012).
- [44] T. Herr, V. Brasch, J. D. Jost, I. Mirgorodskiy, G. Lihachev, M. L. Gorodetsky, and T. J. Kippenberg, *Phys. Rev. Lett.* **113**, 123901 (2014).
- [45] A. B. Matsko, W. Liang, A. A. Savchenkov, and L. Maleki, *Opt. Lett.* **38**, 525 (2013).
- [46] F. C. Cruz, J. D. Marconi, A. Cerqueira S., Jr., and H. L. Fragnito, *Opt. Commun.* **283**, 1459 (2010).
- [47] L. E. Nelson, S. B. Fleischer, G. Lenz, and E. P. Ippen, *Opt. Lett.* **21**, 1759 (1996).
- [48] J. W. Nicholson, F. G. Omenetto, D. J. Funk, and A. J. Taylor, *Opt. Lett.* **24**, 490 (1999).
- [49] D. E. Goldberg, *Genetic Algorithms in Search, Optimization, and Machine Learning* (Addison-Wesley, Reading, MA, 1988).
- [50] A. A. Savchenkov, W. Liang, A. B. Matsko, V. S. Ilchenko, D. Seidel, and L. Maleki, *Opt. Lett.* **34**, 1318 (2009).
- [51] X. Xue, Y. Xuan, Y. Liu, P.-H. Wang, S. Chen, J. Wang, D. E. Leaird, M. Qi, and A. M. Weiner, [arXiv:1406.1116](https://arxiv.org/abs/1406.1116).
- [52] A. Hasegawa, *IEEE J. Sel. Top. Quantum Electron.* **6**, 1161 (2000).